

PLANETARY NEBULAE AS STANDARD CANDLES. III. THE DISTANCE TO M81

GEORGE H. JACOBY AND ROBIN CIARDULLO

Kitt Peak National Observatory, National Optical Astronomy Observatories

HOLLAND C. FORD¹

Johns Hopkins University and Space Telescope Science Institute

AND

JOHN BOOTH

Kitt Peak National Observatory, National Optical Astronomy Observatories

Received 1988 December 28; accepted 1989 March 1

ABSTRACT

We present the results of a survey for planetary nebulae in the nearby Sb galaxy M81 (NGC 3031). Using the Kitt Peak 4 m telescope and a TI CCD, we identify 185 planetary nebula candidates. Photometry of the nebulae extends nearly 2.5 mag below the brightest candidate, although the sample is statistically homogeneous and complete for only 88 nebulae representing the top 1.2 mag of the luminosity function.

We follow the methods outlined by Ciardullo *et al.* in 1989 for using the distinctive shape of the planetary nebula luminosity function to derive extragalactic distances. After correcting for a foreground extinction of $E(B-V) = 0.10$, we derive the distance to M81 to be 3.50 ± 0.40 Mpc. This distance compares very well with values derived using traditional methods such as Cepheids (3.30 Mpc), red supergiants (3.2 Mpc), and the infrared Tully-Fisher relation (3.73 Mpc).

M81 provides an excellent test case for comparing the distances derived from planetary nebulae with estimates using other techniques. It is a relatively nearby galaxy so that other stellar indicators can still be used. Furthermore it has an intermediate Hubble type, thereby allowing the use of late-type indicators (brightest stars, Cepheids, Tully-Fisher) while still permitting the unambiguous identification of numerous planetary nebulae. Based on the excellent agreement among the various distance techniques and the high degree of precision offered by the method, we conclude that planetary nebulae are as good as, or better than, other standard candles for deriving distances to galaxies beyond 10 Mpc.

Subject headings: galaxies: distances — galaxies: individual (M81) — luminosity function — nebulae: planetary

I. INTRODUCTION

Ford and Jenner (1979) made the first attempt to derive a distance to M81 (NGC 3031) using planetary nebulae (PN) as a standard candle. At that time, the available instrumentation limited their observations to the identification of only eight PN candidates. Consequently their derived distance, a factor of 3.5 times farther than M31 (2.5 to 2.8 Mpc), contained a large uncertainty.

Jacoby (1989; Paper I) and Ciardullo *et al.* (1989; Paper II) discuss the shape of the planetary nebula luminosity function (PNLF) and how it can be used to determine reliable extragalactic distances with high accuracy. Paper I shows that one can expect an upper limit to a PN's [O III] $\lambda 5007$ flux, and that the shape of the PNLF can be reproduced solely from theoretical stellar evolutionary tracks and model nebulae. Thus the brightest PN in a galaxy can serve as a standard candle. Paper II investigates in detail the observed shape of the PNLF in M31 and describes the numerical procedures required to derive accurate extragalactic distances (including statistical uncertainties) relative to M31 from prescribed samples of PN observations.

PN offer a number of advantages as standard candles over the alternatives which are commonly used to derive distances to galaxies between 1 and 15 Mpc (Paper I; Paper II). For

instance, as we will show for M81, PN in the central bulge are relatively unaffected by reddening internal to the galaxy and are easily visible in narrow-band images despite the bright galaxy continuum. Furthermore, the narrow-band filters suppress the contribution from the brightest stars which in broad-band images produce a crowded condition requiring an exacting photometric analysis.

M81 offers several advantages over other northern galaxies for comparing PN distances with distances based on more traditional candles. For example, although PN are found in galaxies of all Hubble types, galaxies much later than M81 (type Sb) have many H II regions, small central bulges, and heavy dust lanes, all of which make PN distance measurements difficult. Galaxies much earlier than M81, however, contain few bright Cepheid variables with which to make a reliable distance comparison. In addition, M81 is sufficiently close so that PN can be easily identified and is so similar to M31 that any systematic effects in the method (e.g., chemical composition differences) will not enter into the relative distance determination.

This paper, the third in a series describing the use and testing of PN as standard candles, will show that the PN derived distance to M81 is in very good agreement with distances derived from other methods, indicating that the external consistency of the method is excellent. Paper IV (Ciardullo, Jacoby, and Ford 1989) will discuss another critical test of the method by comparing the derived distances to three galaxies in a single group. The nearly perfect agreement in the distances to galaxies of different Hubble types (NGC 3377-E6, NGC

¹ Visiting Astronomer, Kitt Peak National Observatory, operated by the Association of Universities for Research in Astronomy, Inc., under contract with the National Science Foundation.

3379—E0, and NGC 3384—SB0) observed in the Leo I group implies superb internal consistency for the PN based distances. These two papers provide the basis for future studies deriving distances beyond 10 Mpc.

We describe our imaging techniques and selection criteria for identifying PN in § II. In § III, we discuss the reduction procedures and the random and systematic errors associated with each step. In § IV, we choose a homogeneous sample of PN and determine a distance to M81 by comparing the observed PNLF to a model based both on stellar evolution considerations (Paper I) and on observations of PN in M31 (Paper II). In § V, we evaluate the errors in this distance and compare our results with those of other investigators.

II. OBSERVATIONS AND IDENTIFICATIONS

The central bulge of M81 was observed on the nights of 1985 April 13 and 15 at the prime focus of the Kitt Peak 4 m telescope. The TI2 CCD was used in an on-chip binning mode such that four physical pixels were read as one pixel having dimensions on the sky of 0".6. The total field of view was 4' on a side and is illustrated in Figure 1 (Plate 10).

The observing technique was based on an on-band/off-band procedure developed for narrow band CCD imaging (Ford *et al.* 1988; Paper II). PN were identified using an on-band [O III] $\lambda 5007$ filter having a central wavelength of $\lambda 5002$ to match the heliocentric systemic velocity of -55 km s^{-1} for M81 (Humason, Mayall, and Sandage 1956), and a full width at half-maximum (FWHM) bandpass of 30 Å in the $f/2.77$ converging beam of the telescope (see § IIIc). For comparison, off-band images were obtained through a filter centered on 5298 Å and having a FWHM of 327 Å. The total exposure through the on-band filter was 1.5 hr and consisted of three 30 minute frames. The total exposure through the off-band filter was 18.75 minutes and consisted of five frames.

The outer parts of the 4' field extended beyond the central bulge, and so some contribution from the disk component of M81 was included in the field. To guard against confusion with H II regions, we also obtained a series of on-band/off-band frames centered at H α . Using a 75 Å wide filter centered at 6563 Å, six frames of 10 minutes each plus one frame of 15 minutes were taken of M81's central bulge. Similarly, six frames of 2.5 minutes each were taken through an H α off-band filter centered at 6180 Å and having a FWHM of 348 Å.

We identified PN according to the following criteria which we believe to be conservative in the sense that only *bona fide* PN were included in the sample. To be considered a PN, an object (1) must appear on *each* of the three on-band [O III] frames, (2) must be absent from all of the [O III] off-band and H α off-band frames, (3) must have a stellar point spread function (PSF), and (4) must be very weak or absent from the H α on-band frames. While the first criterion may appear to be overly conservative as it eliminates many of the fainter PN, it effectively guards against confusion with radiation events.

We identified the PN by "blinking" the on-band [O III] sum (Fig. 2 [Pl. 11]) against the off-band sum. Each candidate was examined to be certain that the four criteria were satisfied. We also found it valuable to create a picture which represents the difference between the on-band sum and the off-band sum. By subtracting the continuum of the galaxy, the contrast of emission-line objects was significantly enhanced. More importantly, the rapidly varying background of the galaxy was greatly flattened, thereby improving the subsequent photometry by reducing the difficulty in estimating the local "sky"

values underlying each PN (see § III). Figure 3 (Plate 12) displays the difference picture. This can be compared to its parent image shown in Figure 2.

We began with a preliminary list of 193 PN candidates which satisfied the first three criteria. Upon a detailed examination, we found that one of these objects was identified twice, one was too faint to be reliably identified, and six objects were reclassified as H II regions on the basis of having strong H α emission (criterion 4). The remaining 185 PN candidates are shown in Figure 3 and listed with their coordinates in Table 1. In Table 2 we give coordinates for several stars in the field to be used as offset stars when setting a telescope on the PN.

Coordinates of the PN were derived in a two-step procedure. First 15 SAO stars were identified on a direct plate of M81 taken by T. Kinman at the 2.1 m telescope and used to determine the positions of 10 stars in the CCD field. These field stars were then used to fix the coordinate system for the PN. We estimate that the errors in the absolute coordinates of the PN in Table 1 are less than 1", and the errors in the relative coordinates are less than 0".5.

III. PHOTOMETRY

The photometric results provide the basis for generating the PNLF which, in turn, is used to derive the distance to M81. They are also used to estimate the magnitude level at which incompleteness effects begin to appear in the survey. Below we detail the steps required to calculate the PN magnitudes.

a) Reductions to Instrumental Magnitudes

We have found in previous studies (Paper II, for example) that the accuracy of the PN measurements is improved if the difference picture is used rather than the on-band picture. We chose to follow the same approach for M81. As evidenced by Figure 3, the PN are all isolated objects. Had we observed closer to the nucleus, or had M81 been at a much larger distance, crowded field photometry procedures may have been necessary. Instead one can use relatively simple aperture photometry techniques such as the Mountain Photometry Code (MPC) described by Adams *et al.* (1980). To test this assumption, we derived magnitudes using both aperture photometry (developed by H. Butcher) and point-spread function fitting (DAOPHOT; developed by Stetson 1987) techniques for the PN and a collection of artificial stars which we placed in the field.

Using the tools within the DAOPHOT system (Stetson 1987), we generated 500 artificial stars and added their images onto the difference picture of M81 (Fig. 3). The stars span a 3 mag range overlapping the top 3 mag of the PNLF. Fourteen of these stars fell within 25" of M81's center, a region where saturation begins to occur, and were consequently discarded. Three were too close to bad columns to be measured reliably, and 113 fell so close to other objects that the results from the aperture photometer were not usable. In addition, 19 were too bright to be of interest. The resulting error distribution, binned into 0.25 mag intervals, is given in Table 3 for the remaining 351 stars.

Over the first 2 mag, there was only marginal evidence that the PSF technique yields superior results. Within the last mag, however, the PSF results indicated a distinct advantage over the aperture photometry routines. It would appear that the greater complexity of the PSF method did indeed offer a reward. However, we urge that these results not be taken too literally. The artificial star generator within DAOPHOT

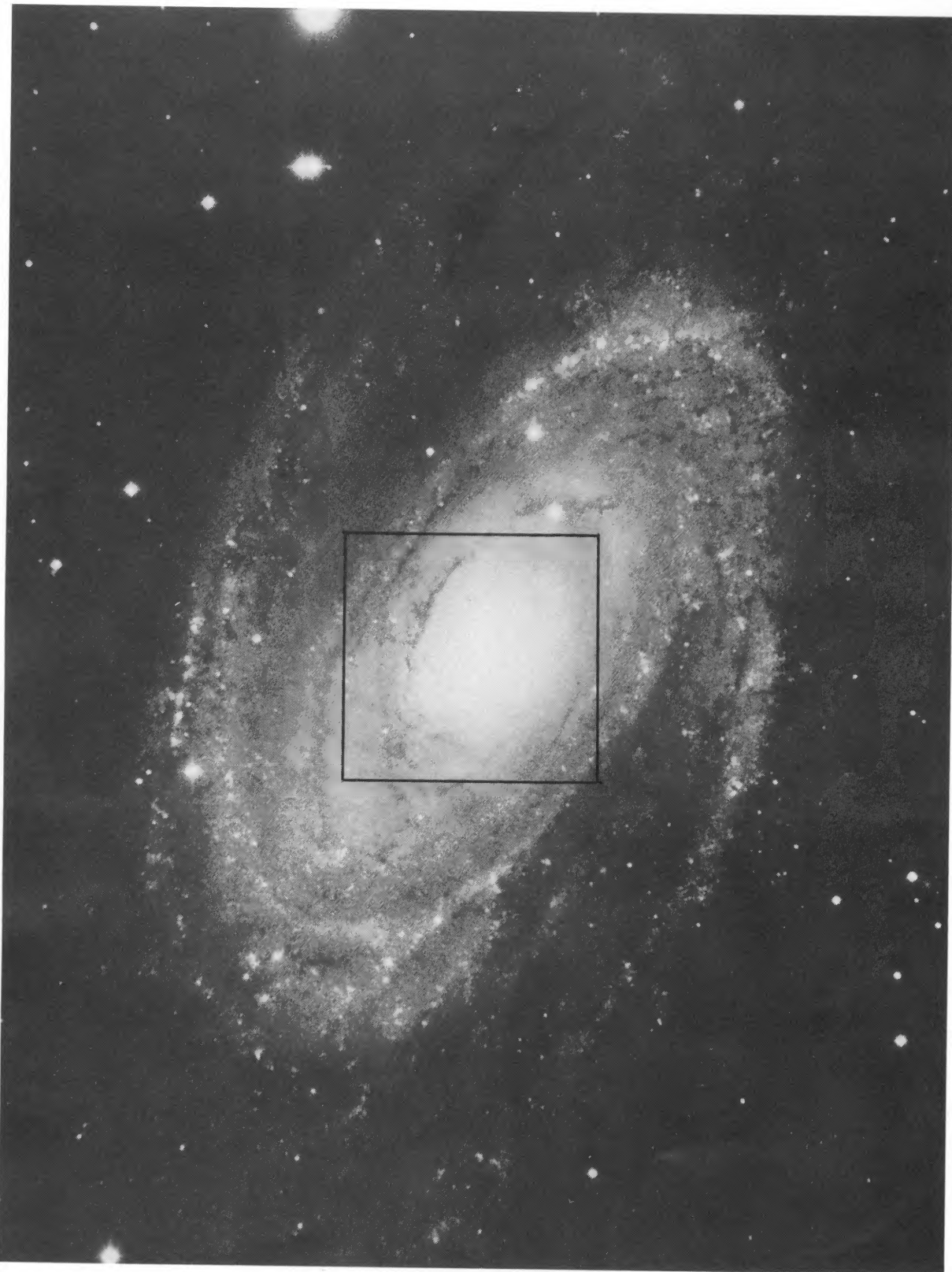


FIG. 1.—A reproduction from the Hubble Atlas (Sandage 1961) showing the 4' field surveyed for PN. South is to the top and east to the right.

JACOBY *et al.* (see 344, 705)

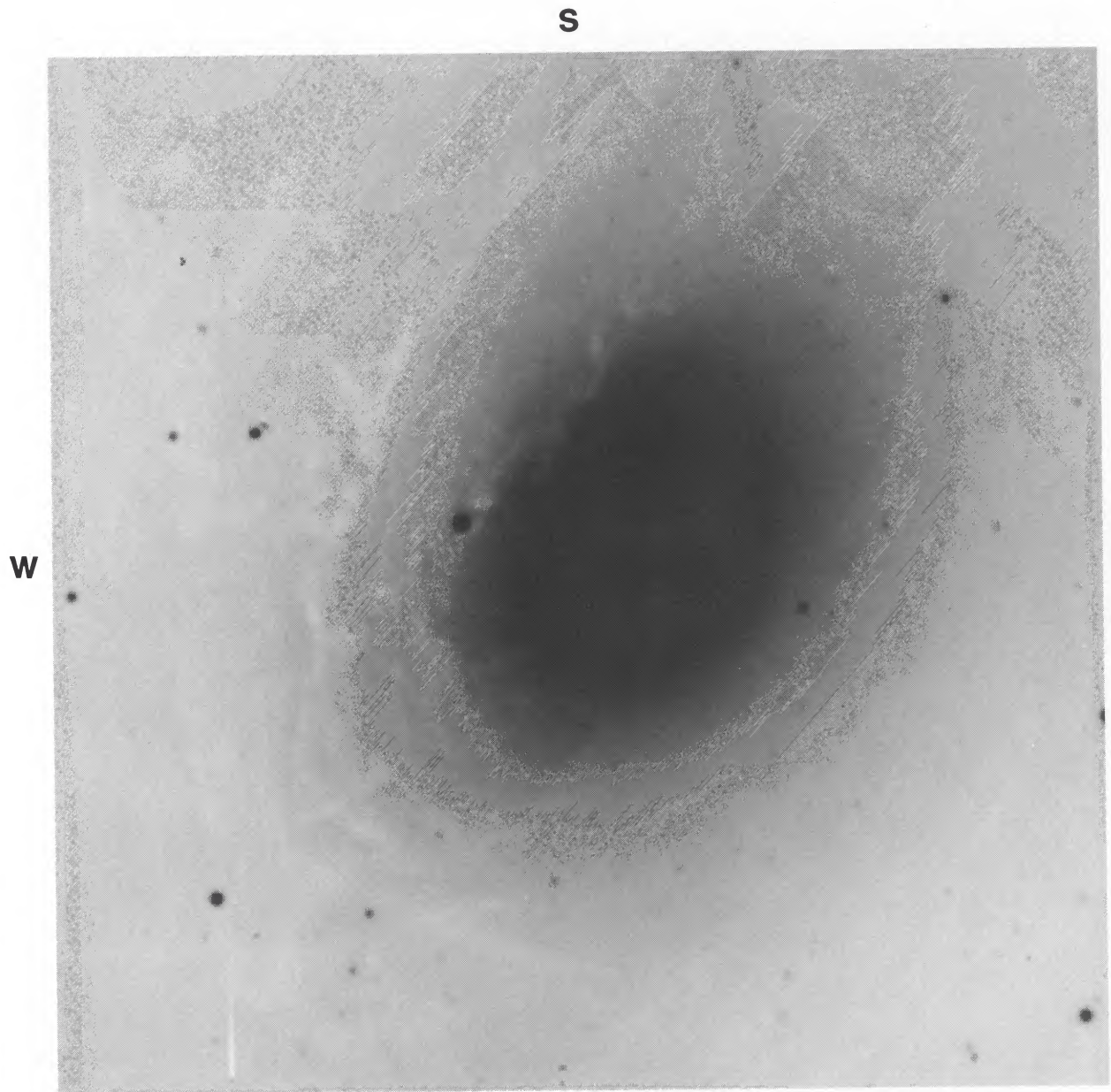


FIG. 2.—The sum of the three on-band [O III] $\lambda 5007$ CCD frames taken with the KPNO 4 m telescope. The effective integration time for this image is 1.5 hr.

JACOBY *et al.* (see 344, 705)

S

W

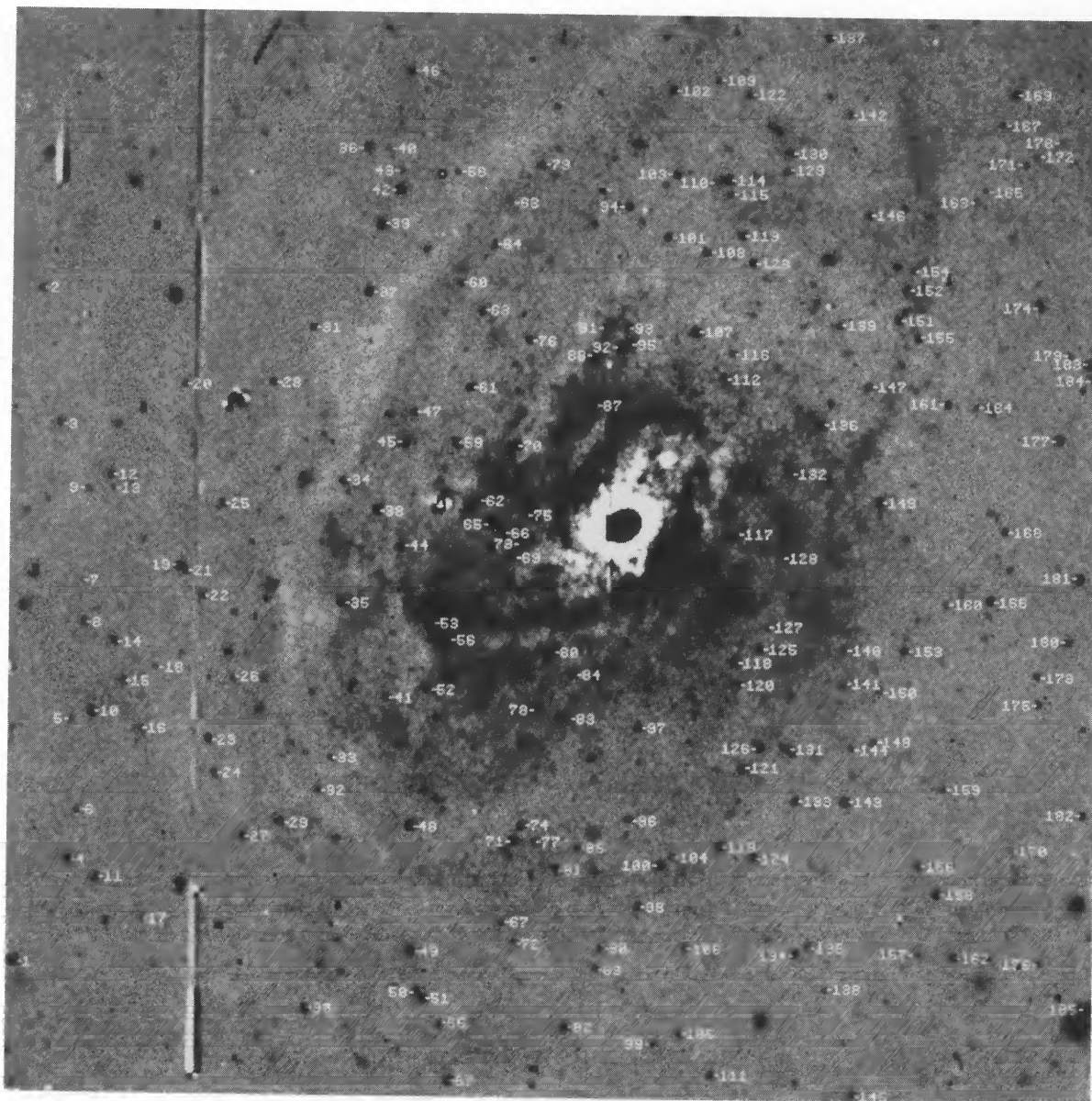


FIG. 3.—The difference picture constructed by subtracting the off-band sum of five images from the on-band sum of three images. The PN candidates are labeled in increasing RA order. Notice how much easier the PN are to see as compared to Fig. 2. Also there is clearly a distinct residual indicating large-scale emission having morphology similar to that seen in M31 by Ciardullo *et al.* (1988).

JACOBY *et al.* (see 344, 705)

TABLE 1
POSITIONS AND APPARENT MAGNITUDES FOR M81 PLANETARY NEBULAE

ID	$\alpha(1950)$	$\delta(1950)$	m_{5007}	Sample	ID	$\alpha(1950)$	$\delta(1950)$	m_{5007}	Sample
1	9 51 03.02	69 19 43.4	23.90	S	49	9 51 19.00	69 19 40.4	24.22	S
2	9 51 03.99	69 17 17.7	25.17		50	9 51 19.21	69 19 49.3	24.48	S
3	9 51 04.78	69 17 46.7	24.81		51	9 51 19.51	69 19 50.7	24.34	S
4	9 51 05.19	69 19 21.2	24.41	S	52	9 51 19.57	69 18 43.7	24.52	S
5	9 51 05.30	69 18 50.9	25.50		53	9 51 19.72	69 18 29.2	24.15	S
6	9 51 05.53	69 19 10.7	25.24		54	9 51 19.92	69 16 52.0	24.38	S
7	9 51 05.70	69 18 20.8	25.80		55	9 51 20.17	69 19 56.2	25.00	
8	9 51 05.77	69 18 30.0	25.23		56	9 51 20.37	69 18 33.0	24.23	S
9	9 51 05.93	69 18 00.9	25.43		57	9 51 20.56	69 20 08.5	24.02	S
10	9 51 06.16	69 18 49.2	24.37	S	58	9 51 20.56	69 16 51.4	25.57	
11	9 51 06.29	69 19 25.2	24.65	S	59	9 51 20.66	69 17 50.1	24.22	S
12	9 51 06.82	69 17 57.8	24.92		60	9 51 20.74	69 17 15.4	24.98	
13	9 51 06.93	69 18 00.4	26.02		61	9 51 21.17	69 17 37.9	24.47	S
14	9 51 07.00	69 18 33.9	24.69	S	62	9 51 21.55	69 18 02.3	24.42	S
15	9 51 07.35	69 18 42.5	25.11		63	9 51 21.64	69 17 21.5	24.73	
16	9 51 08.01	69 18 52.9	25.45		64	9 51 22.09	69 17 07.1	24.96	
17	9 51 08.17	69 19 33.7	25.32		65	9 51 22.10	69 18 07.5	23.87	S
18	9 51 08.64	69 18 39.4	25.71		66	9 51 22.53	69 18 09.9	24.42	S
19	9 51 09.57	69 18 17.7	24.39	S	67	9 51 22.63	69 19 34.0	25.27	
20	9 51 09.75	69 17 38.0	25.01		68	9 51 22.71	69 16 57.6	25.33	
21	9 51 09.83	69 18 18.7	25.14		69	9 51 22.97	69 18 14.7	24.39	S
22	9 51 10.50	69 18 24.1	25.10		70	9 51 23.03	69 17 50.5	23.64	S
23	9 51 10.80	69 18 54.9	24.63	S	71	9 51 23.13	69 19 16.4	24.35	S
24	9 51 11.05	69 19 02.3	25.02		72	9 51 23.14	69 19 38.3	25.18	
25	9 51 11.31	69 18 03.7	25.07		73	9 51 23.37	69 18 11.9	24.00	S
26	9 51 11.76	69 18 41.6	25.49		74	9 51 23.43	69 19 13.0	24.42	S
27	9 51 12.23	69 19 15.7	24.32		75	9 51 23.48	69 18 05.7	24.18	S
28	9 51 13.28	69 17 37.3	24.87		76	9 51 23.51	69 17 27.5	24.56	S
29	9 51 13.70	69 19 12.8	24.64	S	77	9 51 23.94	69 19 16.5	24.88	
30	9 51 14.76	69 19 53.3	24.42	S	78	9 51 23.94	69 18 47.9	24.63	S
31	9 51 14.85	69 17 25.4	24.85		79	9 51 23.94	69 16 49.7	24.61	S
32	9 51 15.23	69 19 05.7	25.16		80	9 51 24.59	69 18 35.1	23.86	S
33	9 51 15.70	69 18 58.7	25.07		81	9 51 24.77	69 19 22.3	24.71	
34	9 51 16.11	69 17 58.5	24.64		82	9 51 25.24	69 19 56.7	24.48	S
35	9 51 16.12	69 18 25.0	24.09	S	83	9 51 25.25	69 18 49.6	24.65	S
36	9 51 16.95	69 16 46.5	25.05		84	9 51 25.42	69 18 39.9	24.50	S
37	9 51 17.08	69 17 17.6	24.04	S	85	9 51 25.67	69 19 17.8	25.32	
38	9 51 17.50	69 18 04.7	24.15	S	86	9 51 26.19	69 18 58.0	24.37	S
39	9 51 17.56	69 17 02.9	24.01	S	87	9 51 26.23	69 17 41.4	23.78	S
40	9 51 17.81	69 16 46.6	25.82		88	9 51 26.26	69 17 30.8	24.16	S
41	9 51 17.88	69 18 45.3	24.96		89	9 51 26.52	69 19 43.7	25.02	
42	9 51 18.30	69 16 55.4	24.00	S	90	9 51 26.70	69 19 39.4	25.24	
43	9 51 18.34	69 16 51.2	25.71		91	9 51 26.69	69 17 24.6	24.45	S
44	9 51 18.49	69 18 12.9	24.51	S	92	9 51 27.29	69 17 29.2	24.06	S
45	9 51 18.60	69 17 49.9	24.04	S	93	9 51 27.52	69 17 24.8	24.59	S
46	9 51 18.68	69 16 30.0	24.87		94	9 51 27.52	69 16 58.4	24.56	S
47	9 51 18.88	69 17 43.5	24.66	S	95	9 51 27.58	69 17 28.6	24.05	S
48	9 51 18.94	69 19 13.4	23.65	S	96	9 51 27.79	69 19 11.4	24.88	

simply replicated the known PSF but at a scaled level, whereas the PSF of a real star includes an additional noise component due to photon noise. Thus DAOPHOT realized a small advantage over the aperture photometer in that the subsequent fit by DAOPHOT is to an exactly known profile. Stetson points out that this advantage is largely of academic interest because the Poisson statistics of the underlying sky will in most cases dominate that of the star when the object is faint.

In any case the superiority of DAOPHOT was only realized in the third mag of the PNLF. We will show in § IVa that the

PNLF is seriously affected by observational incompleteness beyond 1.2 mag, and consequently the choice of reduction techniques is irrelevant. Nevertheless, after having gone through all the procedures, we chose to use the DAOPHOT results.

b) Conversion to Apparent Magnitude

The instrumental magnitudes derived in the previous section were placed on the apparent magnitude scale of Papers I and II

TABLE 1—Continued.

ID	$\alpha(1950)$	$\delta(1950)$	m_{5007}	Sample	ID	$\alpha(1950)$	$\delta(1950)$	m_{5007}	Sample
97	9 51 28.12	69 18 51.6	24.25	S	142	9 51 36.39	69 16 38.0	24.94	
98	9 51 28.20	69 19 30.2	24.81		143	9 51 36.45	69 19 07.1	23.71	S
99	9 51 28.85	69 20 00.1	25.22		144	9 51 36.65	69 18 55.3	25.33	
100	9 51 29.04	69 19 21.3	24.23	S	145	9 51 36.86	69 20 10.5	24.60	S
101	9 51 29.10	69 17 05.0	24.47	S	146	9 51 37.15	69 16 59.8	25.07	
102	9 51 29.22	69 16 33.2	24.53	S	147	9 51 37.24	69 17 36.8	24.62	S
103	9 51 29.43	69 16 51.3	24.66		148	9 51 37.57	69 18 53.9	24.90	
104	9 51 29.56	69 19 19.4	25.38		149	9 51 37.73	69 18 02.0	24.06	S
105	9 51 29.88	69 19 57.8	25.10		150	9 51 37.81	69 18 42.8	25.09	
106	9 51 30.08	69 19 38.9	24.99		151	9 51 38.39	69 17 22.1	24.30	S
107	9 51 30.27	69 17 25.5	23.78		152	9 51 38.73	69 17 15.7	24.56	S
108	9 51 30.67	69 17 08.2	24.71		153	9 51 38.78	69 18 34.0	24.79	
109	9 51 31.04	69 16 31.1	25.18		154	9 51 38.98	69 17 11.3	25.37	
110	9 51 31.07	69 16 52.7	25.01		155	9 51 39.18	69 17 26.1	24.65	S
111	9 51 31.17	69 20 06.7	24.87		156	9 51 39.42	69 19 20.8	24.94	
112	9 51 31.43	69 17 35.6	24.08	S	157	9 51 39.46	69 19 39.6	25.27	
113	9 51 31.46	69 19 17.1	24.42	S	158	9 51 40.18	69 19 26.7	24.20	S
114	9 51 31.52	69 16 52.3	24.07	S	159	9 51 40.40	69 19 04.0	25.20	
115	9 51 31.58	69 16 55.6	24.99		160	9 51 40.41	69 18 23.8	25.34	
116	9 51 31.74	69 17 29.9	24.78		161	9 51 40.41	69 17 40.3	24.74	
117	9 51 31.92	69 18 09.0	24.12	S	162	9 51 40.91	69 19 40.2	24.78	
118	9 51 32.02	69 18 36.9	24.63	S	163	9 51 41.46	69 16 56.4	25.47	
119	9 51 32.07	69 17 04.3	24.70		164	9 51 41.54	69 17 40.8	25.31	
120	9 51 32.09	69 18 41.6	24.54	S	165	9 51 41.82	69 16 53.8	25.55	
121	9 51 32.29	69 19 00.0	24.61	S	166	9 51 42.22	69 18 23.0	24.40	S
122	9 51 32.34	69 16 34.0	24.51	S	167	9 51 42.48	69 16 39.7	25.54	
123	9 51 32.51	69 17 10.4	24.45	S	168	9 51 42.75	69 18 07.6	24.71	
124	9 51 32.80	69 19 19.3	24.30	S	169	9 51 42.99	69 16 33.2	24.13	S
125	9 51 32.96	69 18 34.0	25.16		170	9 51 43.18	69 19 17.0	25.64	
126	9 51 32.99	69 18 55.4	24.17	S	171	9 51 43.38	69 16 48.3	25.40	
127	9 51 33.25	69 18 29.4	25.66		172	9 51 43.91	69 16 46.3	25.76	
128	9 51 33.79	69 18 14.2	25.22		173	9 51 44.10	69 18 39.1	24.79	
129	9 51 33.89	69 16 50.3	25.13		174	9 51 44.10	69 17 19.0	24.65	S
130	9 51 33.94	69 16 46.3	24.78		175	9 51 44.19	69 18 45.1	24.82	
131	9 51 34.07	69 18 55.4	24.22	S	176	9 51 44.34	69 19 41.2	25.16	
132	9 51 34.10	69 17 55.8	24.04	S	177	9 51 44.88	69 17 47.7	24.18	S
133	9 51 34.49	69 19 07.0	24.50	S	178	9 51 44.91	69 16 43.1	26.04	
134	9 51 34.53	69 19 40.1	24.37		179	9 51 45.30	69 17 29.4	24.99	
135	9 51 35.05	69 19 38.3	25.11		180	9 51 45.33	69 18 31.7	24.68	S
136	9 51 35.32	69 17 45.2	24.16	S	181	9 51 45.76	69 18 18.0	23.91	S
137	9 51 35.46	69 16 21.4	24.48		182	9 51 46.02	69 19 09.2	24.85	
138	9 51 35.73	69 19 47.7	25.42		183	9 51 46.08	69 17 31.4	23.86	S
139	9 51 36.03	69 17 23.7	24.56	S	184	9 51 46.25	69 17 34.4	25.28	
140	9 51 36.32	69 18 34.0	25.34		185	9 51 46.34	69 19 50.7	23.88	S
141	9 51 36.33	69 18 41.3	25.28						

TABLE 2
M81 ASTROMETRIC STANDARDS

Star	$\alpha(1950)$	$\delta(1950)$
a.....	9 ^h 51 ^m 09 ^s .65	69°19'27".1
b.....	9 51 11.46	69 17 42.5
c.....	9 51 08.02	69 17 43.1
d.....	9 51 03.73	69 18 19.0
e.....	9 51 20.03	69 18 03.0
f.....	9 51 16.01	69 19 30.7
g.....	9 51 45.91	69 19 54.7
h.....	9 51 45.77	69 17 36.7
i.....	9 51 40.33	69 17 13.4
j.....	9 51 31.69	69 16 20.0

for comparison with the PN absolute magnitudes. This conversion required two adjustments.

First, the DAOPHOT magnitudes were adjusted to account for the fact that not all the stellar flux is included in the PSF fitting procedure. This "aperture correction" was performed by measuring the magnitudes of six isolated stars in the M81 on-band CCD field using the aperture photometry procedures, but through an aperture 5 times larger than the FWHM seeing diameter. The difference in magnitudes between the DAOPHOT values and the large aperture values represents the correction. The average aperture correction for the six stars was 2.391 mag and the standard deviation of the mean was 0.023 mag.

TABLE 3
COMPARISON OF APERTURE PHOTOMETRY RESULTS WITH
DAOPHOT PHOTOMETRY

Magnitude	Stars in Bin	Aperture Photometry Δ^a	DAOPHOT Photometry Δ^a	Fraction of Nondetections
23.50.....	34	0.038	0.029	0.000
23.75.....	29	0.040	0.031	0.000
24.00.....	41	0.056	0.052	0.000
24.25.....	32	0.061	0.057	0.000
24.50.....	28	0.077	0.067	0.000
24.75.....	33	0.108	0.089	0.061
25.00.....	14	0.158	0.147	0.071
25.25.....	24	0.154	0.115	0.083
25.50.....	36	0.166	0.143	0.194
25.75.....	32	0.181	0.165	0.406
26.00.....	34	0.242	0.161	0.500
26.25.....	14	0.344	0.263	0.786

^a Δ is defined as the difference in magnitudes between the derived magnitude of an artificial star and the true value.

This measurement could not have been performed on the difference image where the PN measurements were made because the stars were grossly affected by the continuum subtraction process. Consequently a small additional uncertainty was added due to the difficulty in deriving accurate sky measurements in the rapidly varying background of M81's bulge. Fortunately most of the six stars were reasonably bright and this uncertainty was no larger than 0.03 mag.

With the aperture correction known, the instrumental PN magnitudes were then placed on a standard system. On each night we observed at least two of the following spectrophotometric standard stars: EG 67, EG 129, BD +25°3941, Ross 640, and Feige 34 (Oke 1974; Stone 1977). Magnitudes for these stars were derived using aperture photometry in the same manner as for the aperture correction stars.

We converted the PN instrumental magnitudes to apparent flux using a model for the [O III] $\lambda 5007$ filter transmission (cf. § IIIc) and the procedures for emission-line objects as outlined by Jacoby, Quigley, and Africano (1987). The agreement among the flux to magnitude conversion factors for all the standard stars was typically better than 0.03 mag, and the standard deviation of the mean conversion was 0.017 mag.

Apparent fluxes for the PN were calculated relative to the standard stars and were then converted to apparent [O III] $\lambda 5007$ magnitudes according to the relationship adopted in Papers I and II:

$$m_{5007} = -2.5 \log F_{5007} - 13.74. \quad (1)$$

Magnitudes for the 185 PN identified in M81 are given in Table 1.

c) Corrections to the Filter Transmission Curve

The converging beam from any telescope will alter the transmission properties of an interference filter. If the f-ratio of the telescope is slower (larger) than about f/8, the effects can generally be ignored. However, the prime focus of the KPNO 4 m telescope has an f/2.77 beam, producing ray angles as large as 10°. Consequently the effects of the convergent beam are severe (Eather and Reasoner 1969) and must be properly included.

The convergent beam impinging on the filter can be thought of as a series of concentric annular rings of light. Each ring is associated with a given cone angle. Each cone angle gives rise

to a particular filter transmission curve which can be measured in the laboratory by tilting the filter by exactly the angle of the cone. The equivalent transmission curve for the filter can be computed from the sum of all the individual transmission curves where each curve is weighted by the area of the annulus appropriate to the cone angle. We have that

$$T_\lambda = \frac{\int_{\theta_{\min}}^{\theta_{\max}} T_\lambda(\theta) dA(\theta)}{\int_{\theta_{\min}}^{\theta_{\max}} dA(\theta)}, \quad (2)$$

where θ is the angle of the incoming beam, λ is the wavelength at which the transmission of the filter is to be determined, T is the transmission of the filter, and A is the area of the annulus at angle θ . We define θ_{\min} and θ_{\max} to be the minimum and maximum cone angles that impinge on the filter.

The value for θ_{\min} is nonzero because the central shadow from the secondary support structure of the telescope blocks the low angle light. For the KPNO 4 m, the central obscuration has a diameter of 0.41 of the diameter of the primary so that $\theta_{\min} = 4^\circ 3'$.

If L is the distance between the filter and the focal plane, then over the small angles we need to consider the relative area of the annulus can be approximated by

$$dA(\theta) = 2\pi L^2 \theta d\theta, \quad (3)$$

which when combined with equation (2) gives

$$T_\lambda = \frac{2}{\theta_{\max}^2 - \theta_{\min}^2} \int_{\theta_{\min}}^{\theta_{\max}} \theta T_\lambda(\theta) d\theta. \quad (4)$$

In order to measure the [O III] $\lambda 5007$ filter transmission in the convergent beam, we placed the filter in a Perkin-Elmer Lambda 9 spectrophotometer. A depolarizing optic supplied by Perkin-Elmer was used to remove polarization arising from the illumination of interference filters with nonincident light. Spectra were taken with the filter tilted at angles of 0° through 11° at 1° increments with respect to the incoming f/13 beam. The 12 spectra were then numerically interpolated and integrated. Figure 4 shows both the transmission curves for the

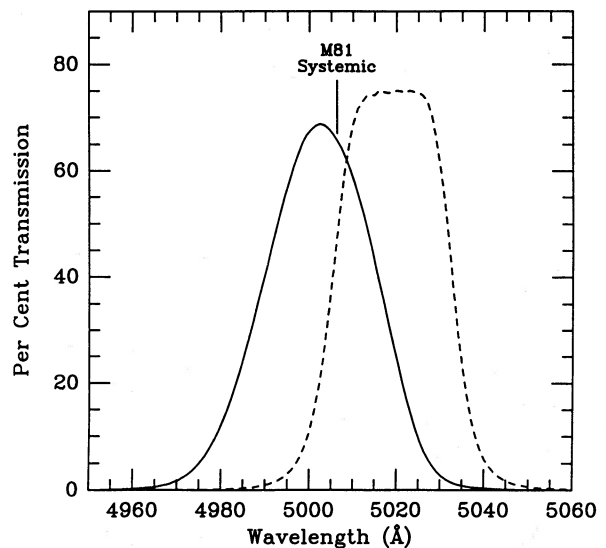


FIG. 4.—The transmission curve for the [O III] $\lambda 5007$ filter used in this survey. The dashed line represents the filter transmission in f/13 light in the laboratory. The solid line is a model for the transmission at 7° C in an f/2.77 beam with a 4°3' obstruction (the secondary mirror and support structure). The systemic velocity of M81 is marked.

filter in a nearly parallel beam and the numerical simulation described by equation (4).

As a test of these procedures, we placed the filter in the KPNO coude feed spectrograph. Light from a continuum lamp entered the spectrograph slit through an $f/32$ beam, was reimaged to $f/2.77$, passed through the filter, and then reimaged back to $f/32$. Since the camera of the spectrograph possesses a central obstruction similar to that at the 4 m, this experiment is consistent with both the numerical recipe and the original observing conditions. The observed spectrum of the filter was then divided by a second spectrum taken with the filter removed from the beam (i.e., a flat-field spectrum). The result represents the filter transmission curve and is nearly indistinguishable from the curve derived using the numerical simulation process. Central wavelengths and bandpasses agreed to within 1 Å, corresponding to an uncertainty in the flux calibration of about 4%. It is difficult to improve this calibration any further. Ideally, we wish to obtain a spectrum through the filter while at the 4 m prime focus, but this is presently not possible.

An additional complication to the filter calibration is that interference filters experience a wavelength shift as a function of ambient temperature. Typically this shift is on the order of +1 Å per +5°C. We monitored the telescope dome temperature during all observations and applied appropriate corrections to the filter transmission curve.

The final factor we consider in deriving PN magnitudes in M81 is the velocity dispersion and rotation in the galaxy's bulge. Stars in the central regions of M81 move at ~ 150 km s^{-1} (Pellet and Simien 1982); therefore there is an intrinsic uncertainty in any individual PN magnitude due to the uncertainty in where the [O III] $\lambda 5007$ line falls along the filter transmission curve. While it is possible in principle (and practice) to measure the velocities of the PN, we do not at this time know this information. Thus, there is a distribution about the mean systemic wavelength of M81, having a dispersion of about ± 2.5 Å. This corresponds to a further random error of +7.5, -4.0% in the PN luminosities. The error is asymmetric because the systemic velocity of M81 falls just to the red of the filter peak. Hence negative moving PN have velocities near the peak, or flat part, of the curve while positive moving PN slide down the shoulder of the transmission curve. (Note that the luminosity of a PN *increases* if the emission falls at a low transmission point since the filter correction would then be large.)

We removed the systematic error introduced by the asymmetry in the following manner. We convolved a Gaussian distribution representing the velocity dispersion of M81's bulge with the filter transmission curve. The centroid of this function is the filter-weighted mean for the PN velocities and corresponds to the transmission which removes the bias in the magnitude measurements. (This does not, however, remove the asymmetry from the error distribution.) This wavelength is 0.1 Å lower than the M81 systemic velocity. The uncertainty in the transmission for a PN, on average, is 5%.

d) Interstellar Extinction to M81

An additional correction to the observed fluxes of PN in M81 is necessary to account for the effects of interstellar extinction. As we shall see, the uncertainties discussed above are largely random and therefore their importance is diminished by the statistical procedures which follow. The remaining systematic errors (e.g., the filter transmission curve effects in an $f/2.77$ beam) are actually small in comparison to the uncer-

tainty in estimating the proper correction for extinction due to dust in the direction of M81.

We assume that the extinction consists of two components: one which is foreground and one which is internal to M81. Two arguments lead us to believe that this latter component has a negligible effect on the PN we find in M81's bulge. (1) As we have seen for M31 (Paper II), and as we will see in the Leo I group (Paper IV), the distribution of PN is identical to that of the stars. Consequently the scale height for PN in the bulge of M81 is large compared to the expected scale height for the dust component, and PN on the near side of M81 should be unaffected by dust. Therefore the objects which contribute most significantly to the distance determination, those PN populating the upper end of the PNLF, are the brightest and least extinguished. (2) Color maps of the bulge of M81 (Fig. 5 [Pl. 13]) illustrate that there are no significant gradients across the field except where dust lanes are present and obvious. We exclude any PN from our sample which happen to fall in these regions (see § IVa).

Similar arguments have been made by Ford and Ciardullo (1988) with respect to novae in M31. They find that the distribution in the maximum magnitude versus rate of decline relation is unchanged after rejecting novae which happen to fall in regions where dust lanes are evident. Since novae, like PN, follow the stellar light distribution in the bulge of M31 (Ciardullo *et al.* 1987), they conclude that these objects suffer little, if any, extinction. By analogy with novae in M31, the situation for PN in the bulge of M81 is likely to be comparable.

Kaufman *et al.* (1987) give an excellent review of the various estimates found in the literature for the foreground extinction to M81. They find that the most probable value is $A_V \approx 0.3$ mag, corresponding to $E(B-V) \approx 0.1$, which is what we adopt here. For completeness, we note that their H II region data, which include a component of the internal extinction, has a mean value of $A_V \approx 1.1 \pm 0.4$ mag. In addition, other estimates for the foreground extinction, A_V , extend from 0.1 (Burstein and Heiles 1984) to 0.6 (Bruzual, Peimbert, and Torres-Peimbert 1982; Peimbert and Torres-Peimbert 1981), although some fraction (about half) of the latter value is attributed to internal extinction. Assuming a Seaton (1979) reddening law, we have $A_{5007} = 3.56E(B-V)$, or 0.36 mag, with an estimated uncertainty in this value of 0.2 mag. We note that this uncertainty could be reduced considerably if the extinction to the individual PN were determined using the ratio of observed to theoretical Balmer decrements. This observation is well within the capabilities of current instrumentation but has not yet been performed. Note that if the extinction to each PN were known, the analysis in the following section would be greatly simplified.

IV. THE DISTANCE TO M81

a) Defining the Complete Sample of PN

In order to derive a distance using the PNLF matching scheme described in Paper II, it is necessary to define a statistically complete sample. We first exclude all PN which may be affected by dust. Following the technique outlined in Paper II, we construct a color map (Fig. 5) from our two off-band images taken through the $\lambda 5300$ ("green" or G) and $\lambda 6200$ ("red" or R) filters. Because our CCD field size is much smaller than the galaxy diameter, we must remove the additive contribution from the sky prior to dividing the green frame by the red frame. We approximate this value by iteratively subtrac-

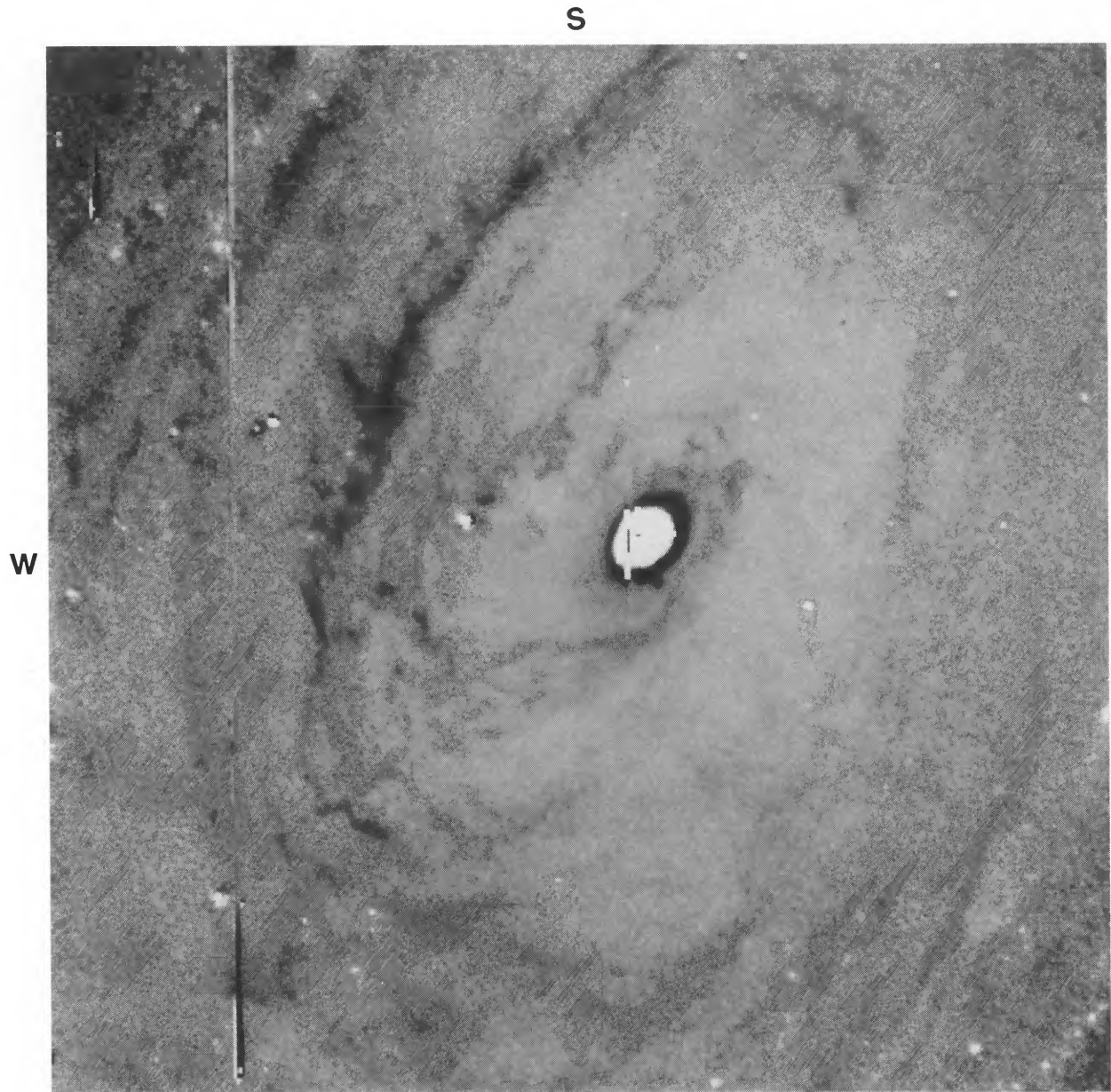


FIG. 5.—A reproduction of the $G-R$ color map for the bulge of M81. The range of colors shown (black to white) corresponds to a color of 0.15 mag.

JACOBY *et al.* (see 344, 709)

ting estimates for the sky levels and comparing the resultant color gradients with the photometry of Brandt, Kalinowski, and Roosen (1972) which show no appreciable gradient. We then vary the sky levels until the derived gradients are minimized.

Following Paper II, we adopt the thin dust layer model in which the near half of the galaxy is unaffected by internal dust, and the far side of the galaxy suffers the full impact of extinction. For a dust cloud having an intrinsic $E(B-V)$ of 0.45 mag, the $G-R$ color excess is 0.08 mag compared to surrounding regions where no dust clouds exist. Any additional dust only makes the area appear bluer because the contribution from the starlight behind the cloud is reduced, and the color of the foreground stars dominates.

The criterion we used in Paper II to identify heavily obscured locations was to reject PN which fall in areas having a $B-\lambda 6200$ color excess of 0.025 mag. This corresponds to a $G-R$ color excess of only 0.012 mag. Unfortunately, this is not much different from the errors we expect from flat-fielding variations and photon statistics. A histogram showing the frequency of *relative* colors (no zero point has been determined) is shown in Figure 6. Since there is no mechanism to generate colors bluer than average, we use the blue-side falloff of this distribution to estimate the uncertainty in the colors. The probable error in the color measurement is found to be 0.020 mag. We therefore adopt the criterion that a PN is rejected if it falls in an area having a $G-R$ excess greater than 0.032 (0.012 + 0.020) mag. Nine PN are eliminated from the sample as a result of this analysis.

We can accentuate faint structures due to dust using a digital unsharp masking technique as described in detail in Paper II. This procedure locates eight additional PN which may be seen through dust; we exclude these from the sample.

As an aside, we see from Figure 5 that the dust in M81 extends as close to the nucleus as we can see before our CCD images saturate ($10''$ or ~ 170 pc). The patterns are also highly reminiscent of the emission and dust morphology seen in M31 (Jacoby, Ford, and Ciardullo 1985; Ciardullo *et al.* 1988). Furthermore, the $G-R$ color excess in the most extreme dust lanes is 0.10 mag, exceeding the maximum value of 0.08 allowed by

the thin layer model. We can understand this excess if the dust lane is above the plane of the disk of M81 so that it obscures more than half of the column along the line of sight. Using the thin dust layer model, we calculate that the fraction of the column which is obscured must be 65%, assuming that the dust introduces the maximum possible color excess. This is, however, inconsistent with the surface brightness of the galaxy at these positions, which would be reduced by 55% according to the model. The actual reduction in surface brightness, about 45%, implies a column fraction close to 50%. Alternatively, the dust could be entirely in front of M81 if it introduces a moderate color excess $E(B-V)$ of 0.16. Clearly, the number of possible configurations is infinite, but at least we are able to restrict the range of parameters.

While we must consider the effects of dust on our sample, the effects of observational incompleteness have a much greater impact on the shape of the PNLF. This is largely due to varying detection limits across the field arising from the sharply increasing galactic background near the center of the field. To investigate this incompleteness, we begin with a histogram of the raw PNLF (Fig. 7) in which the brightest PN have m_{5007} near 23.5. As we progress to fainter magnitudes, PN are more and more numerous until incompleteness becomes important at $m_{5007} > 24.7$. This selection of objects, however, is drawn from an inhomogeneous sample and therefore the shape of the distribution is altered, rendering it unsuitable for deriving an accurate distance. In particular, some of the PN are seen against the bright galaxy background near the nucleus of M81 where faint PN are difficult to detect, thereby raising the apparent frequency of bright PN.

Paper II uses a theoretical technique to calculate the effects of the background galaxy on PN detection limits. The method which was outlined by Ciardullo *et al.* (1987) relies on a knowledge of the telescope system throughput to calculate anticipated signal-to-noise ratios and detection limits across the field. In addition to this procedure, two experimental approaches are also available to assist in defining the completeness cutoff. The first takes advantage of the photometric testing described in § IIIa in which artificial stars are added to the M81 image. If we define nondetection as the case where

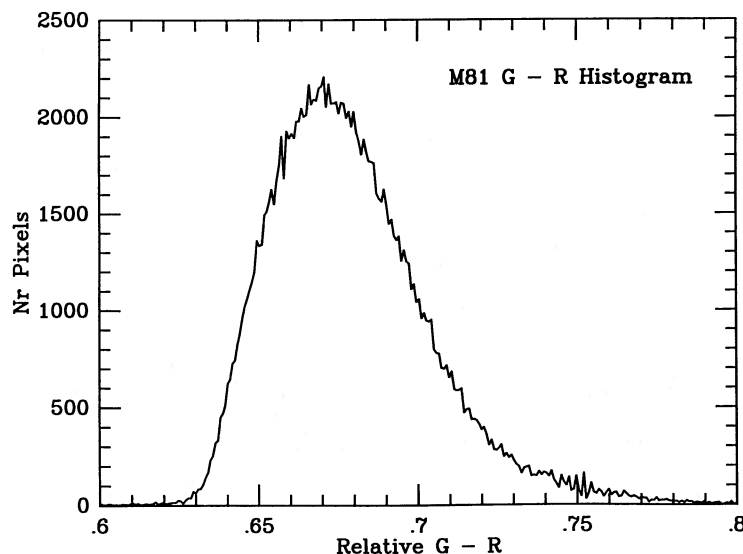


FIG. 6.—The distribution of the $G-R$ colors for all the pixels in Fig. 5. These colors are instrumental, not absolute, and so only relative differences are meaningful.

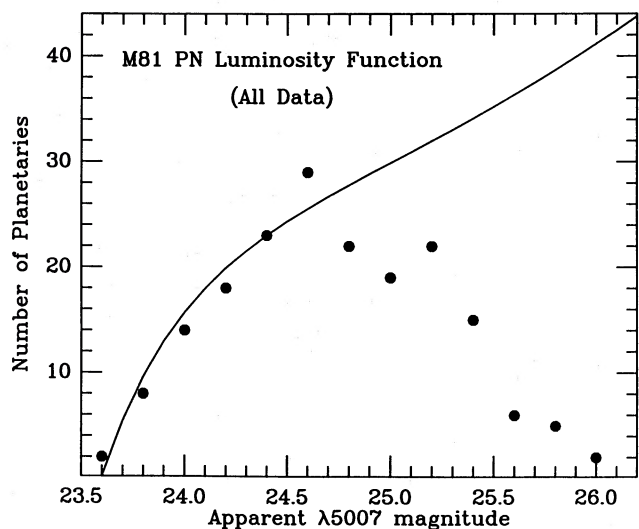


FIG. 7.—The raw PNLF for M81 displayed in 0.2 mag bins. The decrease in the number of PN with $m_{5007} > 24.7$ is due to incompleteness.

either the star cannot be recovered or the photometric error is greater than 0.25 mag, then we can compute the fraction of nondetections as a function of artificial star magnitude. The magnitude for which this fraction becomes significant is the magnitude at which incompleteness begins.

The fraction of nondetections is given in the last column of Table 3. We see that the sample is complete for at least one magnitude ($m_{5007} < 24.75$) and is clearly incomplete after 2.25 mag ($m_{5007} > 25.75$) when the fraction of nondetections exceeds 40%. We tentatively estimate that the point where incompleteness begins is between 1 and 1.5 mag along the PNLF.

The second experiment which we can perform to define the incompleteness limit is to examine the spatial distribution of

PN. Stellar evolution theory predicts that the number of PN per unit galaxy bolometric luminosity is nearly invariant to a stellar population's age or initial mass function (Renzini and Buzzoni 1986). This was confirmed for the bulge and inner disk of M31 (Paper II) and this constancy can be used in the following way.

We compute the ratio of PN to surface luminosity in M81 using the identifications in Table 1 and the photometry from Brandt, Kalinowski, and Roosen (1972). We then choose a limiting magnitude and note at what position along the major axis this ratio begins to drop due to the failure to find PN against the bright galactic background. There will exist some magnitude for which no drop occurs (except, of course, at the very center of the galaxy where the detector saturates), and we can adopt this magnitude as the completeness limit. This occurs for PN brighter than 1.2 mag along the PNLF (see Fig. 8a), or $m_{5007} < 24.7$, in excellent agreement with the artificial star experiment.

On the other hand, we can choose a deeper limit, and eliminate all PN from our sample which are closer to the nucleus than the point (in surface brightness) at which the ratio drops. From Figure 8b, we see that for $m_{5007} < 25.2$, the sample is complete for all PN more distant than 72" from the nucleus. While this sample rejects numerous PN near the nucleus of the galaxy, it includes many at fainter magnitudes, and thus the number of PN in both samples is comparable.

While either sample is statistically suitable for matching the PNLF, we prefer to use the brighter sample which suffers smaller photometric errors and contains a greater number of PN at the bright, distance-sensitive, end of the PNLF. Of the 16 PN excluded from the sample based on their locations with respect to the presence of dust, five have $m_{5007} < 24.7$ thereby reducing the statistically complete sample only slightly. The remaining 88 PN included in sample are noted in Table 1 with an "S." If we had selected the fainter sample ($m_{5007} < 25.2$), the sample size would be 94 PN after rejecting objects near dust lanes.

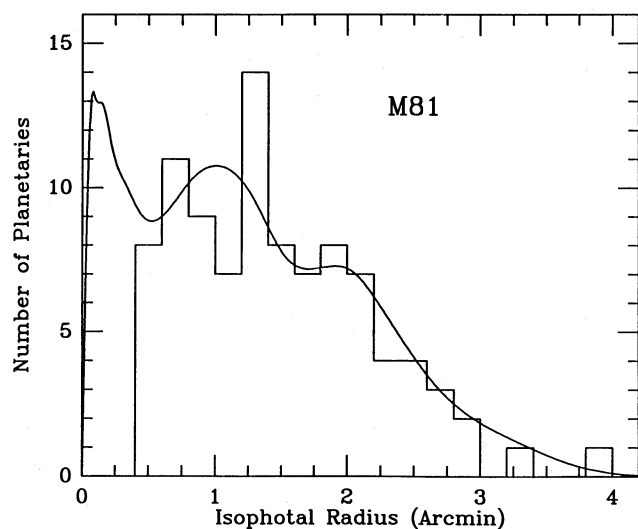


FIG. 8a

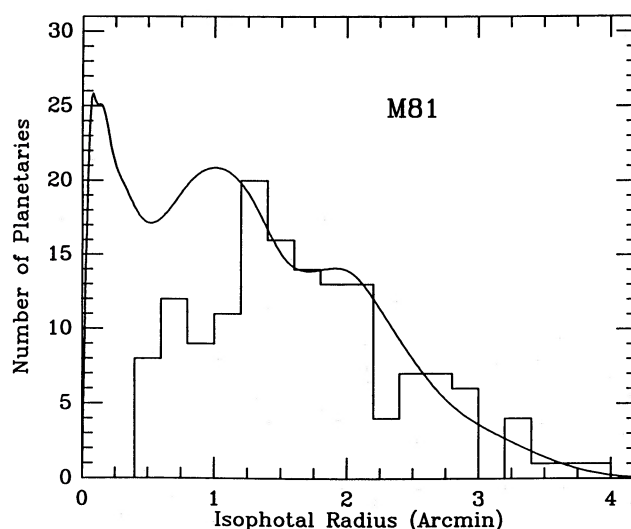


FIG. 8b

FIG. 8.—(a) A histogram showing the distribution of isophotal radii for PN candidates with $m_{5007} < 24.7$. The data have been binned into 12" intervals. The solid line illustrates the amount of luminosity surveyed. Even in the innermost region, no PN are lost. (b) A histogram showing the distribution of isophotal radii for PN candidates with $m_{5007} < 25.2$. The data have been binned into 12" intervals. The solid lines illustrate the amount of luminosity surveyed. The drop in luminosity specific PN density indicates that incompleteness is important at radii less than 72" due to the increasing galaxy background.

b) The PNLF Comparison

In Paper II, we postulated that a luminosity function based on a modified Henize and Westerlund (1963) evolutionary law provided a good fit to the observed distribution in M31. As can be seen in Figure 9, the PN in M81 also obey this law. Based on this excellent agreement, we contend that a good analytic representation of the true distribution is

$$N(M) \propto e^{0.307M} [1 - e^{3(M^* - M)}], \quad (5)$$

where $M^* = -4.48$ and represents the maximum attainable [O III] $\lambda 5007$ luminosity for a PN. By treating this law as a probability distribution, we can compute a distance to M81 which maximizes the likelihood that the homogeneous sample of PN is drawn from this distribution in a random manner.

Before performing this fit, we must convolve the photometric error as a function of magnitude (from Table 3) with the relation specified by equation (5). This accounts for the fact that although the PNLF may be constant from galaxy to galaxy the observed PNLF is the convolution of the true function with the observational error profile. Another potential source of observational error is merging of PN images due to crowding, which, if ignored, would distort the PNLF and reduce the derived distances. This may be important for observations of PN in the cores of galaxies at Virgo-distances, but need not be considered for M81 (see Fig. 3).

One of the results of the fitting process is an estimate for the total number of PN in M81. If we also have an estimate of the total bolometric luminosity for the galaxy, we can make a direct comparison between the observed and predicted stellar death rates. We normalize the total number of PN to the luminosity of M81 using the surface photometry from Brandt, Kalinowski, and Roosen (1972) to compute the total B and V luminosities [after dereddening by $E(B-V) = 0.1$] encompassed in the survey region. We estimate the bolometric correction by assuming that M81 is so similar to M31 (Spinrad and Taylor; Bruzual, Peimbert, and Torres-Peimbert 1982; Fabbiano 1988) that the correction of -0.80 mag for the bulge of M31 (Paper II) is appropriate to the bulge of M81.

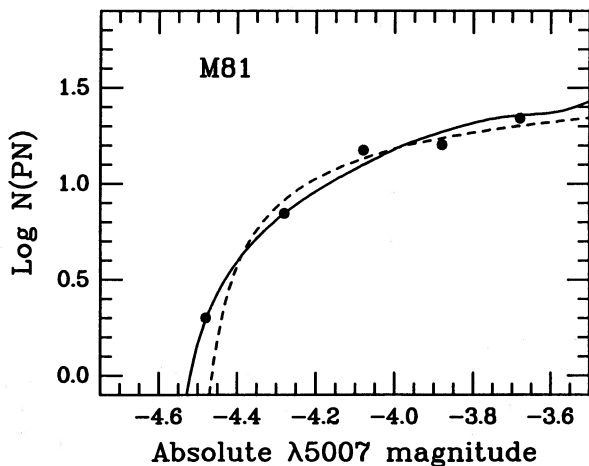


FIG. 9.—A log plot of the M81 PNLF derived from the homogeneous sample of 88 PN. The data have been transformed to an absolute magnitude scale using the extinction and distance discussed in the text. The solid line is the theoretical PNLF computed in Paper I; the dashed line represents the empirical law of eq. (5). Both curves have been convolved with the photometric error function from Table 3.

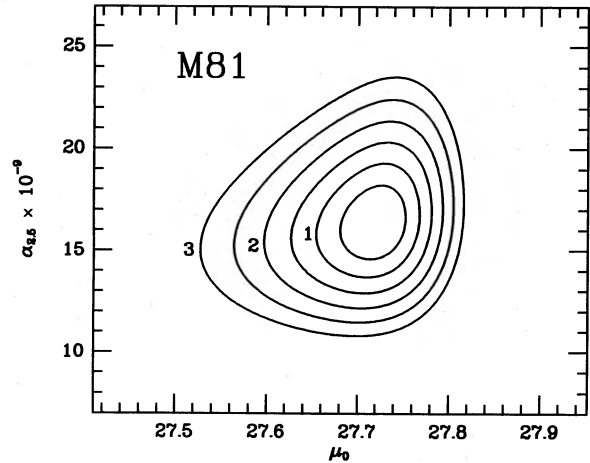


FIG. 10.—Maximum likelihood confidence level contours for M81 derived from the homogeneous sample of PN and assuming the model PNLF described by eq. (5). The plane of the contours is the true distance modulus μ_0 and the number of PN within 2.5 mag of M^* normalized to the bolometric luminosity of the region sampled. Contours are shown at 0.5σ intervals. One, two, and three σ contours are labeled and correspond to confidence levels of 68%, 95%, and 99.5%. The best fit for M81 is at $\mu_0 = 27.72$.

We derive the maximum likelihood solutions to the PNLF using the methods outlined in Paper II. These results are shown in Figure 10. Probability contours are displayed at intervals of 0.5σ in the plane defined by true distance modulus, μ_0 , and bolometric luminosity specific PN density within 2.5 mag of M^* , $\alpha_{2.5}$. We see that the peak of the contours falls at $\mu_0 = 27.72$, $\alpha_{2.5} \times 10^9 = 16.2$, and that the 1σ uncertainties in these values are $+0.05$, -0.07 mag and ± 3 respectively. Even at the 3σ confidence level, the distance modulus for M81 is defined by the PNLF fitting technique to within $+0.10$, -0.20 mag, representing remarkably tight limits for extragalactic distances. Note that the 1σ uncertainty in μ_0 corresponds to an uncertainty in distance of only 3%!

We also note that our value for $\alpha_{2.5}$ is in very good agreement with the value of $11 \pm 2 \times 10^{-9}$ found for M31. The implied stellar death rate for M81, after extrapolating $\alpha_{2.5}$ using equation (5) over the 8 mag range of the entire PNLF implied by a typical lifetime of 25,000 yr (Pottasch 1984), is $\sim 8.4 \times 10^{-12}$ stars $\text{yr}^{-1} L_{\odot}^{-1}$. This is a factor of 3 smaller than predicted by Renzini and Buzzoni (1986), but the considerable extrapolation of the observations, the presence of dust which inhibits detection of some PN and requires rejection of others from the sample, and the unknown details relating PN formation rates and stellar death rates, introduce comparable uncertainty.

The preliminary values for μ_0 (27.74) and $\alpha_{2.5}$ (17.7×10^{-9}) presented by Jacoby, Ciardullo, and Ford (1988) differ in that the [O III] $\lambda 5007$ filter characteristics have been reevaluated to include the effects of the telescope central obstruction, and the surface brightness profile for M81 has been more precisely modeled.

V. DISCUSSION

We find the distance modulus for M81 to be 27.72 with impressively small internal errors. The sample of PN is sufficiently large that the random errors which we discussed in § III almost insignificant. We are, however, still plagued by systematic errors. As noted earlier, the most troublesome term is due to extinction. Most other methods of distance determination

TABLE 4
COMPARISON OF DISTANCES TO M81

Source	Distance Modulus (μ_0)	Distance (Mpc)	Method
Humphreys <i>et al.</i> 1986	27.55	3.25	Red supergiants
Freedman and Madore 1988	27.59 ± 0.31	3.30	<i>I</i> band Cepheids
Bottinelli <i>et al.</i> 1984	27.60 ± 0.16	3.31	<i>B</i> band Tully-Fisher
de Vaucouleurs 1978	27.70 ± 0.3	3.47	Brightest stars, H II
Aaronson, Mould, and Huchra 1980	27.86 ± 0.3	3.73	IR Tully-Fisher
Sandage 1984	28.8	5.75	<i>B</i> band Cepheids
This paper	27.72 ± 0.25	3.50	PN luminosities

are similarly affected by extinction, but less so for those relying on long wavelength observations (e.g., IR Cepheid measurements). When spectroscopic observations of the PN in M81 are obtained, this uncertainty can be reduced to an arbitrarily small value.

A simple test we can perform is to derive the distance to M81 using the sample of PN in which we rejected objects in dusty areas, and also for the sample which includes those objects. The resulting distances are identical. At this time, however, we conservatively choose to carry the 0.2 mag uncertainty.

Another potentially serious systematic error is that we have set our zero point for the PNLF using M31. Two aspects of this deserve consideration. (1) The distance to M31 is not known exactly. (2) Chemical composition differences between M31 and M81 may affect the value of M^* .

While we must accept the inherent uncertainty in the distance to M31, we note that values in the literature (cf. Welch *et al.* 1986; Pritchett and van den Bergh (1987) generally agree to within 5% (0.1 mag).

Regarding the question of composition effects, we recall that the spectra and colors of the bulge components of M31 and M81 are nearly identical, suggesting that abundance differences, if present, are very small. Furthermore, any such variations enter only as a square root dependence (Paper I; Paper IV) into the PN luminosities. We can therefore neglect this consideration from the distance comparison which follows.

In Table 4, we compare our results for the distance to M81 with a broad sampling from the literature. Uncertainties, when given or calculable, are included. Distance estimates for M81 based on a measurement to NGC 2403 have not been included due to the added confusion arising from cluster depth (Aaronson, Mould, and Huchra 1980; de Vaucouleurs 1978). Furthermore, we make no attempt to reconcile different values for the extinction and calibrator zero points in these studies.

The uncertainty in the value from this paper, 0.25 mag, is derived by adding in quadrature the uncertainties in magnitudes for the extinction (0.2), M31's zero point distance (0.1), the value of M^* derived from M31 (0.08), the 1σ statistical uncertainty from Figure 10 (0.07), and the photometric calibration errors due to aperture correction (0.02), standard star transformation (0.02), and filter transmission (0.04). While it would appear that the (somewhat arbitrarily chosen) uncertainty in the value for extinction dominates this calculation, the net uncertainty only drops to 0.18 mag if the extinction uncertainty were reduced by half.

We see that the range in derived distance moduli is generally between $\mu_0 = 27.5$ and $\mu_0 = 27.9$. Our value falls near the middle. In fact, given realistic uncertainties for extinction and zero point values, none of these distances is significantly discrepant. Probably the most reliable result of the group (other than ours) is that derived by Freedman and Madore (1988) using two Cepheids. Their value of $\mu_0 = 27.59 \pm 0.31$ is indistinguishable from our value of $\mu_0 = 27.72 \pm 0.25$.

We conclude that the distance to M81 derived from PN is as accurate as that from any other method. Furthermore, for the special case of M81, PN offer the following advantages. (1) The observations utilize the telescope efficiently in that only one epoch of data is required. (2) PN are sufficiently bright through narrow-band filters so that as a consequence of suppression of the background galaxy light, the photometric accuracy is excellent. (3) Chemical composition effects can be neglected due to similarities with the calibrating galaxy, M31. (4) Since PN follow the distribution of the starlight, the brightest PN, which enter most strongly into the distance determination, are least affected by internal dust.

This paper considers two issues which we feel need to be addressed to provide confidence in our procedure for deriving distances from PN. First, by showing that the PN based distance to M81 agrees with distances derived from other techniques, we prove that the PNLF matching method can yield unbiased distances. Moreover, we demonstrate that the external errors are comparable to, or smaller than, those encountered using the best alternative methods. The internal errors are insignificant in this particular case, but will become more important with greater distances as the shot noise in the PN photometry dominates.

Second, the excellent agreement between the shape of the M81 PNLF and the M31 PNLF (actually, the model based upon it) shown in Figure 9 illustrates the constancy of the PNLF, at least across galaxies of similar Hubble types. In Paper IV we show that this constancy applies to other galaxy types as well, thereby providing the basis for using PN on a wide range of galaxies, and at distances greater than 10 Mpc. We believe that this paper and Paper IV prove conclusively that the PNLF is an excellent distance indicator.

This work was supported in part by NASA grants NAS529293 and NAGW-421.

REFERENCES

- Aaronson, M., Mould, J., and Huchra, J. 1980, *Ap. J.*, **237**, 655.
 Adams, M., Christian, C., Mould, J., Stryker, L., and Tody, D. 1980, *Stellar Magnitudes from Digital Pictures* (Tucson: Kitt Peak National Observatory).
 Bottinelli, L., Gouguenheim, L., Paturel, G., and de Vaucouleurs, G. 1984, *Astr. Ap. Suppl.*, **56**, 381.
 Brandt, J. C., Kalinowski, J. K., and Roosen, R. G. 1972, *Ap. J. Suppl.*, **24**, 421.
 Bruzual, A. G., Peimbert, M., and Torres-Peimbert, S. 1982, *Ap. J.*, **260**, 495.

- Burstein, D., and Heiles, C. 1984, *Ap. J. Suppl.*, **54**, 33.
- Ciardullo, R., Ford, H. C., Neill, J. D., Jacoby, G. H., and Shafter, A. W. 1987, *Ap. J.*, **318**, 520.
- Ciardullo, R., Jacoby, G. H., and Ford, H. C. 1989, *Ap. J.*, **344**, 715. (Paper IV).
- Ciardullo, R., Jacoby, G. H., Ford, H. C., and Neill, J. D. 1989, *Ap. J.*, **339**, 53. (Paper II).
- Ciardullo, R., Rubin, V. C., Jacoby, G. H., Ford, H. C., and Ford, W. K., Jr. 1988, *A.J.*, **95**, 438.
- de Vaucouleurs, G. 1978, *Ap. J.*, **224**, 710.
- Eather, R. H., and Reasoner, D. L. 1969, *Appl. Optics*, **8**, 227.
- Fabbiano, G. 1988, *Ap. J.*, **325**, 544.
- Ford, H. C., and Ciardullo, R. 1988, in *The Extragalactic Distance Scale*, ed. S. van den Bergh and C. J. Pritchett (Provo: Brigham Young University Press), p. 128.
- Ford, H. C., Ciardullo, R., Jacoby, G. H., and Hui, X. 1988, in *IAU Symposium 131, Planetary Nebulae*, ed. S. Torres-Peimbert (Dordrecht: Reidel), p. 335.
- Ford, H. C., and Jenner, D. C. 1979, *Bull. AAS*, **10**, 665.
- Freedman, W. L., and Madore, B. F. 1988, *Ap. J. (Letters)*, **332**, L63.
- Henize, K. G., and Westerlund, B. E. 1963, *Ap. J.*, **137**, 747.
- Humason, M. L., Mayall, N. U., and Sandage, A. 1956, *A.J.*, **61**, 97.
- Humphreys, R. M., Aaronson, M., Lebofsky, M., McAlary, C. W., Strom, S. E., and Capps, R. W. 1986, *A.J.*, **91**, 808.
- Jacoby, G. H. 1989, *Ap. J.*, **339**, 39. (Paper I).
- Jacoby, G. H., Ciardullo, R., and Ford, H. C. 1988, in *The Extragalactic Distance Scale*, ed. S. van den Bergh and C. J. Pritchett (ASP Conference Series No. 4), (Provo: Brigham Young University Press), p. 42.
- Jacoby, G. H., Ford, H., and Ciardullo, R. 1985, *Ap. J.*, **290**, 136.
- Jacoby, G. H., Quigley, R. J., and Africano, J. L. 1987, *Pub. A.S.P.*, **99**, 672.
- Kaufman, M., Bash, F. N., Kennicutt, R. C., and Hodge, P. W. 1987, *Ap. J.*, **319**, 61.
- Oke, J. B. 1974, *Ap. J. Suppl.*, **27**, 21.
- Peimbert, M., and Torres-Peimbert, S. 1981, *Ap. J.*, **245**, 845.
- Pellet, A., and Simien, F. 1982, *Astr. Ap.*, **106**, 214.
- Pottasch, S. R. 1984, *Planetary Nebulae: A Study of Late Stages of Stellar Evolution* (Dordrecht: Reidel), p. 215.
- Pritchett, C. J., and van den Bergh, S. 1987, *Ap. J.*, **316**, 517.
- Renzini, A., and Buzzoni, A. 1986, in *Spectral Evolution of Galaxies*, ed. C. Chiosi and A. Renzini (Dordrecht: Reidel), p. 195.
- Sandage, A. 1961, in *The Hubble Atlas of Galaxies* (Washington, DC: Carnegie Institution), atlas page 19.
- Sandage, A. 1984, *A.J.*, **89**, 621.
- Seaton, M. J. 1979, *M.N.R.A.S.*, **187**, 73p.
- Spinrad, H., and Taylor, B. J. 1971, *Ap. J. Suppl.*, **22**, 445.
- Stetson, P. B. 1987, *Pub. A.S.P.*, **99**, 191.
- Stone, R. P. S. 1977, *Ap. J.*, **218**, 767.
- Welch, D. L., McAlary, C. W., McLaren, R. A., and Madore, B. F. 1986, *Ap. J.*, **305**, 583.

JOHN BOOTH, ROBIN CIARDULLO, and GEORGE H. JACOBY: Kitt Peak National Observatory, P.O. Box 26732, Tucson, AZ 85726

HOLLAND C. FORD: Space Telescope Science Institute, 3700 San Martin Drive, Baltimore, MA 21218